Intensified Continuous Flow Process for the Scalable Production of Bio-Based Glycerol Carbonate

Claire Muzyka,[a] Sébastien Renson,[a] Bruno Grignard,[b],[c] Christophe Detrembleur,[b] and Jean-Christophe M. Monbaliu*[a]

[a] C. Muzyka, S. Renson, Prof. Dr. J.-C. M. Monbaliu
Center for Integrated Technology and Organic Synthesis (CiTOS), MolSys Research Unit, University of Liège
Address: Allée du Six Août 13, B-4000 Liège (Sart Tilman), Belgium
E-mail: jc.monbaliu@uliege.be | www.citos.uliege.be

[b] Dr. B. Grignard, Dr. C. Detrembleur
Center for Education and Research on Macromolecules (CERM), CESAM Research Unit, University of Liège
Address: Allée du Six Août 13, B-4000 Liège (Sart Tilman), Belgium

[c] Dr. B. Grignard
Federation of Researchers in Innovative Technologies for CO_2 Transformation (FRITCO$_2$T technology platform), University of Liege
Address: Allée de la Chimie, B6a, 4000 Liège, Belgium

Supporting information for this article is given via a link at the end of the document.

Abstract: A subtle combination of fundamental and applied organic chemistry toward process intensification is demonstrated for the large-scale production of bio-based glycerol carbonate under flow conditions. The direct carbonation of bio-based glycidol with CO_2 is successfully carried out under intensified flow conditions, with Barton's base as a potent homogeneous organocatalyst. Process metrics for the CO_2 coupling step (for the upstream production, output: 3.6 kg day^{-1}, Space Time Yield (STY): 2.7 kg h^{-1} L^{-1}, Environmental factor (E-factor): 4.7) outclass previous reports. High conversion and selectivity are achieved in less than 30 s of residence time at pilot scale with a stoichiometric amount of CO_2. Supporting DFT computations reveal the unique features of the mechanism in presence of Brønsted bases.

Ambitious R&D and production directives in Europe now favor the integration of disruptive technologies for reducing the environmental impact, for enhancing safety measures and for lifting the extensive reliance on petro-based chains of value.[1–5] In this context, significant efforts have been dedicated to the upgrading of glycerol (**1**) into industrially relevant bio-based platform compounds, such as glycidol (**2**) and glycerol carbonate (**3**).[5,6] In this context, **3** has rapidly accessed the status of rising star. It has several advantages over other petro-based carbonates such as ethylene and propylene carbonates, which are key electrolyte carriers in lithium batteries.[7] The flammability of **3** is much lower in comparison to ethylene/propylene carbonates, thus significantly reducing the inherent fire hazards associated with Li-based batteries.[8] By condensation with dicarboxylic acids or diacyl chlorides,[8] **3** has also served as a building block for the construction of bicyclic carbonates suitable for non-isocyanate polyurethanes (**NIPU**) by polyaddition with polyamines. However, the use of **3** in **NIPU** chemistry remains marginal.[5,8–15] Carbonate **3** can also be used as a bio-lubricant, formulating agent or alternative green solvent.[5]

The global production of **3** is still limited, estimated to *ca.* 3 Mt y^{-1} in 2020,[16] which most likely relates to the overall inefficiency of current industrial processes.[5] There are currently three main synthetic routes to access **3** (A-C, Figure 1a). [6,17–21] The most economically viable processes feed on activated glycerol derivatives such as **2** and CO_2.

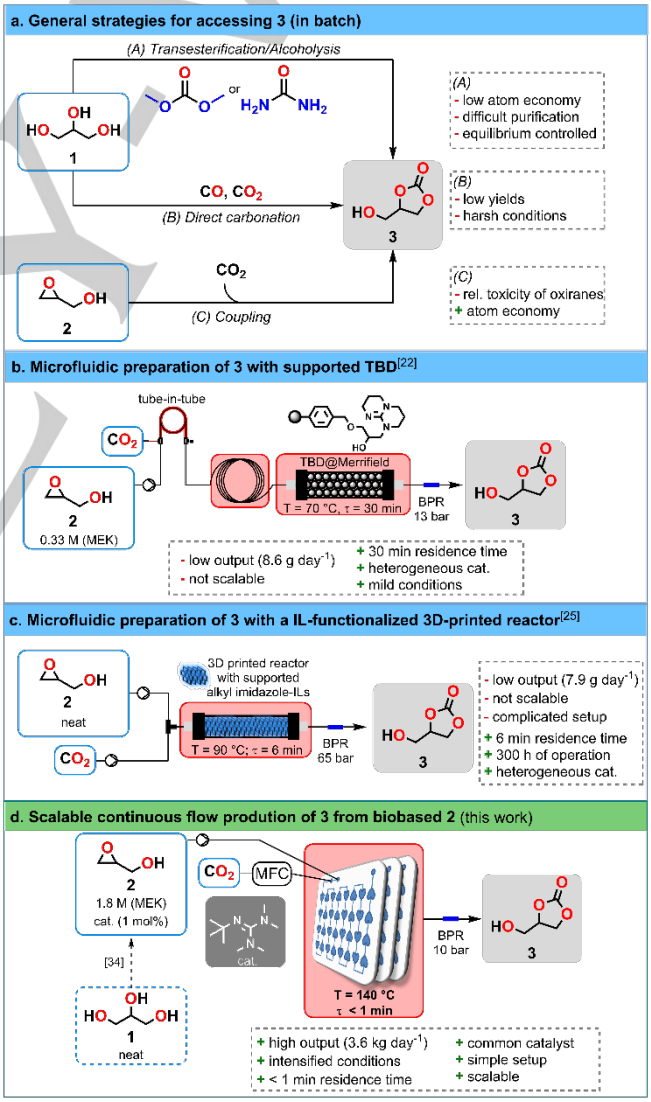

Figure 1. a. Typical preparations of **3** (A: transesterification/alcoholysis of **1**; B: direct carbonation of **1** with CO or CO_2; C: coupling of **2** with CO_2); **b.** Microfluidic preparation of **3** from **2** and CO_2 with a heterogenized catalyst and featuring a tube-in-tube configuration;[22–24] **c.** Microfluidic preparation of **3** from **2** and CO_2 with a 3D-printed reactor;[25] with covalent ionic liquid functionalization; **d.** This

work: scalable and intensified flow preparation of **3** from biobased **2** with a homogeneous catalyst.

However, the alleged inert nature of CO_2 leads to extended reaction times, hampering the global process efficiency.[26–29] Various carbonation protocols using CO_2 on oxiranes with homogeneous and heterogeneous catalysts have been reported under flow conditions,[30–33] among which only two reports specifically disclosed the carbonation of **2** (Figure 1b,c)[22,25] with low overall productivities.

Our previous studies established an intensified and scalable flow process to convert bio-based **1** into the corresponding oxiranes, including **2** with high selectivity (Section S5, Supporting Information).[34] With the invaluable opportunities in terms of scalability, safety and intensification brought by flow process technology,[18,34–39] we sought for further downstream valorization of **2** and for a concrete solution to access **3** at large scale (Figure 1d). We hereby present a DFT-guided homogeneous catalytic process to access carbonate **3**.[35,40] Structure reactivity relationships were established among a library of nitrogen-containing homogeneous organocatalysts displaying a range of pK_{aH} to maximize the reaction selectivity, conversion and output. A DFT study further rationalized the mechanism. These conditions relied on a stoichiometric amount of CO_2, a low catalyst loading and a short residence time with very high conversion and selectivity. The scalability and intensification of the process were validated with favorable metrics (3.6 kg day^{-1}).

To ensure seamless scalability, specific technical and chemical options were selected: CO_2 was fed into the reactor setup with a mass flow controller and homogenous catalysis in 2-butanone (methyl ethyl ketone, MEK) was privileged.[41] 1,5,7-Triazabicyclo[4.4.0]dec-5-ene (**TBD**) was selected as a model catalyst for the direct coupling of gaseous CO_2 with **2**.[22] The influence of temperature, counter-pressure and CO_2 flow rate on the reaction outcome were assessed with 5 mol% of **TBD** in a microfluidic reactor (Figure 2, Section S6.1, Supporting information). The preliminary scouting of reaction conditions led to conditions striking a balance between yield and selectivity under intensified conditions. These conditions involved processing **2** at 140 °C (10 bar) with 2 min of residence time and 10 mL_N/min of gaseous CO_2.

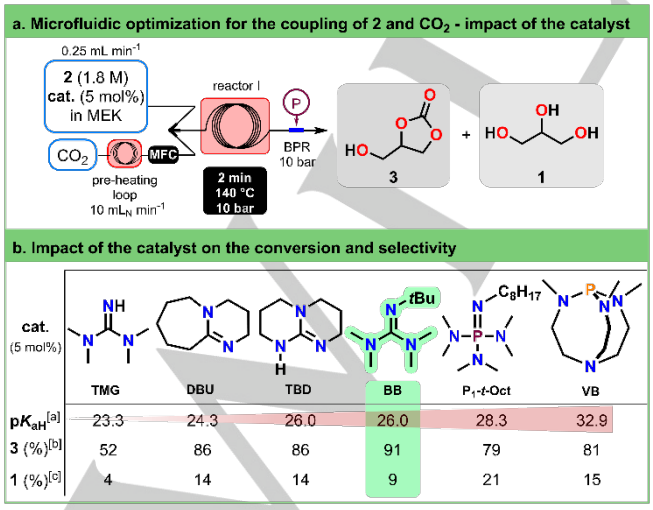

Figure 2. a. Microfluidic prototype for the screening of catalyst. Conditions: **2** (1.8 M in MEK with 5 mol% **cat.**) at 0.25 mL min^{-1}; CO_2 (gas, 1 equiv.) at 10 mL_N min^{-1}, 140 °C, 10 bar, 2 min estimated residence time. MFC = Mass Flow Controller; **b.** Screening of various homogeneous nitrogen-containing organic bases for the coupling of bio-based **2** with CO_2 (see **a.**). [a] Indicative values for experimental pK_{aH} in MeCN reported in the literature[42,43]. [b] Yield in **3** determined by ^{1}H NMR. [c] Yield of **1** determined by ^{1}H NMR.

Next, a library of potential nitrogen-containing homogeneous organocatalysts was investigated. The series of homogeneous organocatalysts (Figure 2b) featured 1,1,3,3-tetramethylguanidine (**TMG**),1,8-diazabicyclo[5.4.0]undec-7-ene (**DBU**), 2-*tert*-butyl-1,1,3,3-tetra- methylguanidine (Barton's base, **BB**), *tert*-octylimino-tris(dimethylamino)phosphorane (**P$_1$-*t*-Oct**), as well as 2,8,9-trimethyl-2,5,8,9-tetraza-1-phosphabicyclo-[3.3.3]undecane (Verkade's base, **VB**). All selected bases were evaluated under standardized process conditions (Section S6, Supporting Information). Starting with the lowest pK_{aH} (e.g., **TMG**, **DBU** and **TBD**), **3** was obtained in up to 86% yield, with the formation of increasing amounts of **1** (up to 14%). **BB** afforded the best compromise with a high yield (91% in **3**) with only a minor amount of **1**. Stronger bases than **BB** (**P$_1$-*t*-Oct** and **VB**) significantly increased the formation of **1**. With **BB** as the most promising catalyst, further optimization eventually led to 82% in **3** with only 1 mol% (Section 6.2, Supporting Information) and a stoichiometric amount of CO_2. Decreasing the catalytic loading to 0.5 and 0.1 mol% drastically decreased the conversion to 53 and 12%, respectively.

The scalability of the process was next evaluated in commercial mesofluidic glass reactors (Corning® Advanced-flow Reactors™, Section S6.5, Supporting Information). Temperatures from 120 to 150 °C (10 bar) were assessed first in a lab scale mesofluidic system with a feed solution of **2** (1.8 M in MEK) and 1 equiv. of CO_2 in the presence of 1 mol% of **BB** (Table 1).

Table 1. Scalability trials for the carbonation of **2** in a mesofluidic lab scale glass reactor of 13.5 mL for various temperature and residence times using 1 mol% of Barton's base (**BB**).

Entry	T (°C)	Residence time (s)	**2** conv. (%)	**3** yield (%)	**1** yield (%)
1	120	50	55	52	3
2	120	70	66	62	4
3	120	140	76	66	10
4	130	50	71	66	6
5	130	70	86	80	6
6	130	140	82	76	6
7	140	50	84	77	6
8[a]	140	70	95	88	7
9[a]	140	54	91	82	8
10[a]	140	41	87	78	9
11[a]	140	27	69	63	6
12[a]	140	13.5	34	31	3
13	140	140	93	85	8
14	150	50	92	85	7
15	150	70	97	88	9
16	150	140	95	88	7

[a] Experiments performed with a liquid flow rate of 1.82 mL min^{-1} and with a gaseous flow rate of 72.9 mL_N min^{-1}.

Comparable trends to the microfluidic experiments were collected: increasing the temperature had a positive impact on the reaction outcome. At 140 °C and 70 s of residence time, **3** was obtained in 88% yield (1 mol% **BB**). A further increase of both the temperature and residence time did not improve the selectivity. At the highest flow rate, implementing 150 °C led to the clogging of the reactor, most likely due to ring opening polymerization of **2**.[44,45] The influence of the residence time independently of the mixing was also studied (Table 1, entries 8-12). A decrease of the residence time had a moderate impact from 70 to 41 s with a loss of 10% yield for **3**, whereas further shortening to 27 s and 13.5 s lowered the yields (63 and 31%, respectively).

Additional data points were considered with **DBU** and **TBD** (1 mol%) under similar conditions. In both cases, clogging of the first fluidic module was observed. **DBU** is known to easily form an adduct with CO_2,[46] which is poorly soluble in most organic solvents. **TBD** was unsuccessful as well, since it triggered the polymerization of **2**,[47] starting at 120 °C. This clogging issue was also observed for the experiment with 1 mol% of **BB** at 150 °C, therefore also underlining the thermal limitation of the reaction with **BB**.

The carbonation process was then carried out in a pilot mesofluidic reactor with **BB** (1 mol%). A representative flow chart is depicted in Figure 3. Further intensification led to conversions of up to 85% within remarkably short residence times (43 s: 80%, 28 s: 78%, 21 s: 67%) at 140 °C. These results simply outperform all conditions reported in the primary literature so far. The attractiveness of this process is emphasized by its high throughput and low footprint, which translates to a Space Time Yield (STY) of 2.7 kg h^{-1} L^{-1} and an E-factor of 4.7 for the upstream carbonation process (Section S6.5.6, Supporting Information).[48] Crude carbonate **3** was purified with a simple liquid-liquid extraction with water (1% NaCl) and methyl isobutyl ketone (MIBK), affording **3** in 71% isolated yield (>95% purity) (Section S7, Supporting Information). The end-to-end process comes with an E-factor of 1.99, provided that MIBK and MEK are recovered through vacuum distillation (Section S6.5.6, Supporting Information).

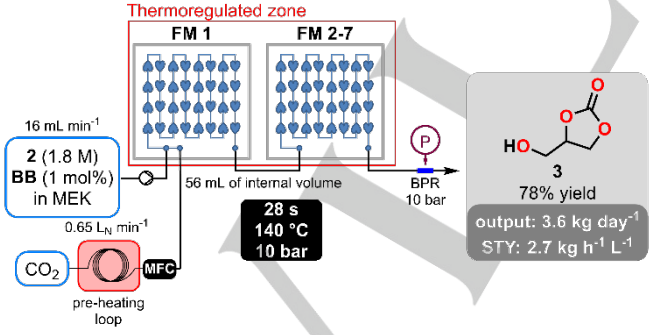

Figure 3. Intensified mesofluidic pilot-scale process (Corning® AFR™ G1, 7 glass fluidic modules in series) for the coupling of **2** and CO_2. Conditions: **2** (1.8 M in MEK with 1 mol% **BB**) at 16.18 mL min^{-1} CO_2 (gas, 1 equiv.) at 648 mL_N min^{-1}, 140 °C, 10 bar, 28 s estimated residence time. FM = Fluidic Module, MFC = Mass Flow Controller. Up to 4% glycerol (**1**) was detected in the crude reactor effluent

Experimental observations highlighted that the β-OH group on **2** plays a critical role, thus suggesting a direct substrate activation with **BB** (Section S9.1, Supporting Information). Indeed, the carbonation of oxiranes lacking a β-OH group, such as epichlorohydrin and *t*-butyl glycidyl ether, gave no conversion. When a 2.25:1 mixture of **2** and epichlorohydrin was subjected to the same conditions, selective coupling occurred with **2**, leaving epichlorohydrin unreacted (Section S6.4.2, Supporting Information). However, by contrast to Kleij's work,[49] the addition of water did not improve CO_2 capture: control experiments under strictly anhydrous conditions gave marginal differences (2-4%) for the conversion to **3**. The potential involvement of a CO_2-adduct with weakly basic nitrogen-containing organocatalysts was also ruled out.[50,51]

The mechanism was studied computationally with the Gaussian 16 software package[52] (Section S9, Supporting Information) for a selection of organocatalysts (**TMG**, **DBU**, **TBD**, **BB** and **P_1-*t*-Oct**). The mechanism (Figure 4a) features two steps: (a) an intermolecular CO_2 capture (step 1) and (b) an intramolecular cyclization toward **3** (step 2).

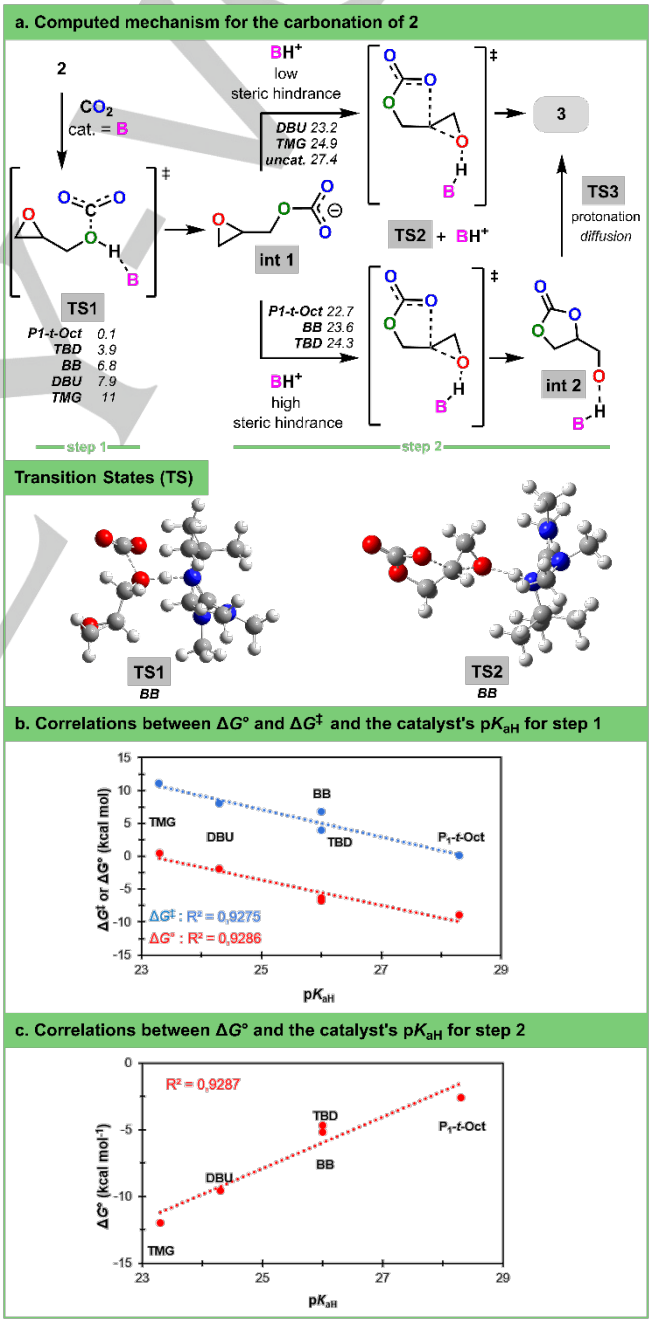

Figure 4. a. Mechanism for the organocatalyzed coupling of CO_2 and **2** toward **3,** computed at the B3LYP-GD3BJ/6-31+G*//M08HX/6-311++G** level of theory (SMD = MEK, 413 K). Activation barriers ($\Delta G^{\ddagger}$) are given in kcal mol^{-1} and mentioned next the acronyms of the various bases. **b.** Free Gibbs energy of reaction ($\Delta G°$, in red) and activation barriers ($\Delta G^{\ddagger}$, in blue) as a function of pK_{aH} of the catalysts for step 1. **c.** Calculated Free Gibbs energy of reaction ($\Delta G°$) for step 2. Experimental pK_{aH} were collected from the literature and measured in MeCN. (Section S9, Supporting Information).

Step 1, which involves the catalyst, the hydroxyl group of **2** and CO_2, leads to **int 1**. It proceeds through low activation barriers ($\Delta G^{\ddagger}$) ranging from 0.1 (**P$_1$-*t*-Oct**) to 11 kcal mol^{-1} (**TMG**) depending on the catalyst, thus indicating a fast CO_2 capture. $\Delta G^{\ddagger}$ can be linearly correlated with the p*K*a of the catalyst (Figure 4b, blue): decreasing $\Delta G^{\ddagger}$ are associated with an increasing Brønsted basicity. Regarding the thermodynamics ($\Delta G°$) of the process, the high stability of CO_2 is overcome with the favorable acid-base reaction at the hydroxyl group of **2**. This assumption is supported by a negative value of $\Delta G°$ for **DBU**, **TBD**, **BB** and **P$_1$-*t*-Oct**, thus ensuring a favorable CO_2 capture, which also correlates with the pK_{aH} of the catalyst (Figure 4b, red).

Step 2 is promoted through the activation of **int 1** by the conjugated acid of the catalyst (produced in step 1) through another proton shuffle. There are, however, two distinct mechanisms depending on the steric hinderance of the catalyst. Catalysts with a lower steric congestion (e.g., **TMG** and **DBU**) directly lead to the final products (**3** and the regenerated active catalytic species). It involves an asynchronous concerted TS, where both the intramolecular cyclization and the proton transfer to the alkoxide occur. Values of $\Delta G^{\ddagger}$ range from 23.2 (**DBU**) to 24.9 kcal mol^{-1} (**TMG**), depending on the catalyst. A change of the mechanism from concerted to stepwise is noticed with highly hindered bases (e.g., **BB** and **P$_1$-*t*-Oct**). The intramolecular cyclization occurs first, where the oxirane ring is activated through H-bonding with the conjugated acid of the catalyst, yielding **int 2**. The latter is then protonated (**TS3**, diffusion-limited) to give **3** with the concomitant recovery of the catalyst. For **TBD**, the stepwise pathway seems to be favored due to the symmetry of its protonated form. The uncatalyzed intramolecular cyclization appeared uncompetitive with a much higher $\Delta G^{\ddagger}$ (27.4 kcal mol^{-1}). Moreover, the presence of the catalyst shifts the equilibrium toward the formation of the products by drastically lowering $\Delta G°$. The thermodynamics of the second step are again dictated by the acid-base equilibrium (Figure 4c).

In summary, a range of nitrogen-containing organocatalysts were assessed experimentally and computationally. Computations emphasized the unique features of a double H-shuffle mechanism for the coupling of CO_2 and glycidol according to a 2-step mechanism. The catalyst's basicity is of paramount importance for step 1. Indeed, a high pK_{aH} ensures a fast and favorable CO_2 fixation with the formation of a highly stable conjugated acid along with a linear carbonate intermediate. Step 2 is drastically accelerated in the presence of the conjugated acid of the catalyst, which acts as a general Brønsted acid catalyst for the activation of the epoxide, though it remains overall rate-determining. Contrasting trends are observed in the activation energies of the two steps of carbonation. This observation provides insight into why Barton's Base emerged with the most favorable results for the entire transformation process. When a stronger base is employed, it leads to a weaker conjugate acid, which in turn acts as a less effective Brønsted acid for the activation of the epoxide. Given the fast kinetics of both steps, the carbonation is likely limited by the solubility of CO_2 in the reaction medium, therefore justifying both the selection of MEK as reaction medium and flow for high mass transfer. The process was validated at the pilot scale in a commercial mesofluidic reactor, affording high yields and selectivity within 28 s with an unprecedented productivity at low catalyst loading (1 mol%). This constitutes a significant improvement of existing conditions toward the intensified and scalable preparation of glycerol carbonate.

Acknowledgements

This research program was funded by the University of Liege, the French Community of Belgium (Concerted Research Action CO2FLUIDICS 21/25-04, PI: CD, co-PI: JCMM), by the European Regional Development Fund (ERDF) and Wallonia within the framework of the program "Wallonie-2020.EU" (INTENSE4CHEM, project under grant No 699993-152208 and 8.1.4/3948 REACT-EU, PI: JCMM). The authors acknowledge the "Fonds de la Recherche Scientifique (F.R.S.-FNRS) for funding (CD is F.R.S.-FNRS Research Director). Computational resources were provided by the Consortium des Équipements de Calcul Intensif (CÉCI), funded by the F.R.S.-FNRS under Grant No. 2.5020.11 and by Wallonia. The manuscript was written through contributions of all authors. All authors have given approval to the final version of the manuscript. The Center for Integrated Technology and Organic Synthesis (CiTOS) incorporates a Corning Application Qualified Laboratory. The authors declare no competing financial interests. Patent application pending.

Keywords: Intensification • Continuous flow • Glycerol carbonate • CO_2 • Bio-based chemicals

[1] "Chemicals strategy," can be found under https://single-market-economy.ec.europa.eu/sectors/chemicals/chemicals-strategy_en, accessed on January 1, 2024.

[2] "Transition pathway," can be found under https://single-market-economy.ec.europa.eu/sectors/chemicals/transition-pathway_en, accessed on January 1, 2024.

[3] "A more robust bioeconomy could help the EU accelerate its progress towards a circular and low-carbon economy," can be found under https://rea.ec.europa.eu/news/more-robust-bioeconomy-could-help-eu-accelerate-its-progress-towards-circular-and-low-carbon-economy-2023-11-27_en, accessed on January 1, 2024.

[4] "Bio-based products," can be found under https://single-market-economy.ec.europa.eu/sectors/biotechnology/bio-based-products_en, accessed on January 1, 2024.

[5] C. Muzyka, J.-C. M. Monbaliu, *ChemSusChem* **2022**, *15*, e202102391.

[6] R. Gérardy, D. P. Debecker, J. Estager, P. Luis, J.-C. M. Monbaliu, *Chem. Rev.* **2020**, *120*, 7219–7347.

[7] E. C. Evarts, *Nature* **2015**, *526*, S93–S95.

[8] M. O. Sonnati, S. Amigoni, E. P. T. De Givenchy, T. Darmanin, O. Choulet, F. Guittard, *Green Chem.* **2013**, *15*, 283–306.

[9] C. Carré, Y. Ecochard, S. Caillol, L. Avérous, *ChemSusChem* **2019**, *12*, 3410–3430.

[10] S. Dabral, T. Schaub, *Adv. Synth. Catal.* **2018**, *361*, 223–246.

[11] S. Gennen, B. Grignard, T. Tassaing, H. Jérôme, C. Detrembleur, *Angew. Chem. Int. Ed.* **2017**, *56*, 10530–10534.

[12] L. Maisonneuve, O. Lamarzelle, E. Rix, E. Grau, H. Cramail, *Chem. Rev.* **2015**, *115*, 12407–12439.

[13] M. Bourguignon, B. Grignard, C. Detrembleur, *Angew. Chem. Int. Ed.* **2022**, *61*, e202213422.

[14] B. Quienne, N. Kasmi, R. Dieden, S. Caillol, Y. Habibi, *Biomacromolecules* **2020**, *21*, 1943–1951.
[15] D. S. Wunschik, K. N. Ingenbosch, M. Zähres, J. Horst, C. Mayer, M. Jäger, V. Strehmel, M. Dornbusch, K. Hoffmann-Jacobsen, *Green Chem.* **2018**, *20*, 4738–4745
[16] G. M. Lari, G. Pastore, M. Haus, Y. Ding, S. Papadokonstantakis, C. Mondelli, J. Pérez-Ramírez, *Energy Environ. Sci.* **2018**, *11*, 1012–1029.
[17] B. Limburg, À. Cristòfol, F. della Monica, A. W. Kleij, *ChemSusChem* **2020**, *13*, 6056–6065.
[18] Z. Wang, R. Gérardy, G. Gauron, C. Damblon, J.-C. M. Monbaliu, *React Chem Eng* **2018**, *4*, 17–26.
[19] R. Gérardy, J. Estager, P. Luis, D. P. Debecker, J.-C. M. Monbaliu, *Catal. Sci. Technol.* **2019**, *9*, 6841–6851.
[20] V. Aomchad, À. Cristòfol, F. della Monica, B. Limburg, V. D'Elia, A. W. Kleij, *Green Chem.* **2021**, *23*, 1077–1113.
[21] J. Poolwong, V. Aomchad, S. del Gobbo, A. W. Kleij, V. D'Elia, *ChemSusChem* **2022**, *15*, e202200765.
[22] N. Zanda, A. Sobolewska, E. Alza, A. W. Kleij, M. A. Pericàs, *ACS Sustain Chem. Eng.* **2021**, *9*, 4391–4397.
[23] C. J. Mallia, I. R. Baxendale, *Org. Process Res. Dev.* **2016**, *20*, 327–360.
[24] L. Yang, K. F. Jensen, *Org. Process Res. Dev.* **2013**, *17*, 927–933.
[25] D. Valverde, R. Porcar, M. Zanatta, S. Alcalde, B. Altava, V. Sans, E. García-Verdugo, *Green Chem.* **2022**, *24*, 3300–3308.
[26] J. A. Castro-Osma, J. Martínez, F. de La Cruz-Martínez, M. P. Caballero, J. Fernández-Baeza, J. Rodríguez-López, A. Otero, A. Lara-Sánchez, J. Tejeda, *Catal. Sci. Technol.* **2018**, *8*, 1981–1987.
[27] J. Rintjema, R. Epping, G. Fiorani, E. Martín, E. C. Escudero-Adán, A. W. Kleij, *Angew. Chem. Int. Ed.* **2016**, *55*, 3972–3976.
[28] Y. Zhang, G. Yang, R. Xie, L. Yang, B. Li, G. Wu, *Angew. Chem. Int. Ed.* **2020**, *132*, 23491–23498.
[29] J. Steinbauer, A. Spannenberg, T. Werner, *Green Chem.* **2017**, *19*, 3769–3779.
[30] D. Rigo, R. Calmanti, A. Perosa, M. Selva, G. Fiorani, *ChemCatChem* **2021**, *13*, 2005–2016.
[31] Y. Wu, Y. Ding, J. Xu, Y. Wang, K. Mumford, G. W. Stevens, W. Fei, *Green Energy Environ.* **2021**, *6*, 291–297.
[32] A. Rehman, A. M. López Fernández, M. F. M. G. Resul, A. Harvey, *J. CO2 Util.* **2018**, *24*, 341–349.
[33] M. R. Li, M. C. Zhang, T. J. Yue, X. B. Lu, W. M. Ren, *RSC Adv.* **2018**, *8*, 39182–39186.
[34] R. Morodo, R. Gérardy, G. Petit, J.-C. M. Monbaliu, *Green Chem.* **2019**, *21*, 4422–4433.
[35] P Bianchi, J.-C. M. Monbaliu, *Angew. Chem. Int. Ed.* **2023**, e202311526
[36] N. N. Tshibalonza, J.-C. M. Monbaliu, *Green Chem.* **2017**, *19*, 3006–3013.
[37] N. N. Tshibalonza, R. Gérardy, Z. Alsafra, G. Eppe, J.-C. M. Monbaliu, *Green Chem.* **2018**, *20*, 5147–5157.
[38] L. Capaldo, Z. Wen, T. Noël, *Chem. Sci.* **2023**, 14, 4230–4247.
[39] N. Kockmann, P. Thenée, C. Fleischer-Trebes, G. Laudadio, T. Noël, *React. Chem. Eng.* **2017**, *2*, 258-280.
[40] Y. Chen, S. Renson, J.-C. M. Monbaliu, *Angew. Chem. Int. Ed.* **2022**, *61*, e202210146.
[41] X. Gui, Z. Tang, W. Fei, *J. Chem. Eng. Data* **2011**, *56*, 2420–2429.
[42] R. Schwesinger, J. Willaredt, H. Schlemper, M. Keller, D. Schmitt, H. Fritz, *Chem. Ber.* **1994**, *127*, 2435–2454.
[43] Ishikawwa T., *Superbases for Organic Synthesis: Guanidines, Amidines and Phosphazenes and Related Organocatalysts*, John Wiley & Sons, Ltd, Chichester, UK, **2009**.
[44] A. Thomas, S. Mü, H. Frey, *Biomacromolecules* **2014**, *15*, 1935–1954.
[45] S. Liu, L. Liu, Y. Zhou, Y. Chen, J. Zhao, *Polym. Chem.* **2022**, *13*, 3650.
[46] M. Lv, P. Wang, Y. Yao, *ChemCatChem* **2016**, *9*, 4451–4455.
[47] L. Simón, J. M. Goodman, *J. Org. Chem.* **2007**, *72*, 9656–9662.
[48] D. J. C. Constable, A. D. Curzons, V. L. Cunningham, *Green Chem.* **2002**, *4*, 521–527.
[49] R. Huang, J. Rintjema, J. González-Fabra, E. Martín, E. C. Escudero-Adán, C. Bo, A. Urakawa, A. W. Kleij, *Nat Catal* **2019**, *2*, 62–70.
[50] C. Maquilón, B. Limburg, V. Laserna, D. Garay-Ruiz, J. González-Fabra, C. Bo, M. Martínez Belmonte, E. C. Escudero-Adán, A. W. Kleij, *Organometallics* **2020**, *39*, 1642–1651.
[51] V. Laserna, E. Martin, E. C. Escudero-Adán, A. W. Kleij, *ACS Catal.* **2017**, *7*, 5478–5482.
[52] Gaussian 16, Revision C.01, M. J. Frisch, G. W. Trucks, H. B. Schlegel, G. E. Scuseria, M. A. Robb, J. R. Cheeseman, G. Scalmani, V. Barone, G. A. Petersson, H. Nakatsuji, X. Li, M. Caricato, A. V. Marenich, J. Bloino, B. G. Janesko, R. Gomperts, B. Mennucci, H. P. Hratchian, J. V. Ortiz, A. F. Izmaylov, J. L. Sonnenberg, D. Williams-Young, F. Ding, F. Lipparini, F. Egidi, J. Goings, B. Peng, A. Petrone, T. Henderson, D. Ranasinghe, V. G. Zakrzewski, J. Gao, N. Rega, G. Zheng, W. Liang, M. Hada, M. Ehara, K. Toyota, R. Fukuda, J. Hasegawa, M. Ishida, T. Nakajima, Y. Honda, O. Kitao, H. Nakai, T. Vreven, K. Throssell, J. A. Montgomery, Jr., J. E. Peralta, F. Ogliaro, M. J. Bearpark, J. J. Heyd, E. N. Brothers, K. N. Kudin,V. N. Staroverov, T. A. Keith, R. Kobayashi, J. Normand, K. Raghavachari, A. P. Rendell, J. C. Burant, S. S. Iyengar, J. Tomasi, M. Cossi, J. M. Millam, M. Klene, C. Adamo, R. Cammi, J. W. Ochterski, R. L. Martin, K. Morokuma, O. Farkas, J. B. Foresman, and D. J. Fox, Gaussian, Inc., Wallingford CT, **2019**.

Entry for the Table of Contents

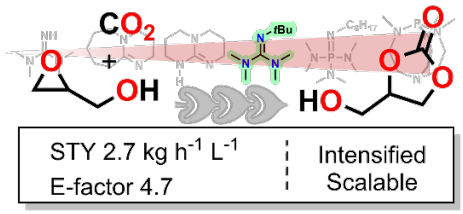

Text for Table of Contents

An intensified continuous flow process for the production of glycerol carbonate from bio-based glycidol and stoichiometric CO_2 in the presence of a homogeneous organocatalyst. It features an unprecedented mechanism and fast CO_2 capture rate, which set robust foundations for large scale operation.

Institute and/or researcher Twitter usernames: @UniversiteLiege @ULiegeRecherche @JMonbaliu, @s_renson_

ORCID numbers: Claire Muzyka 0000-0002-6133-8449; Sébastien Renson 0000-0002-4721-8635; Bruno Grignard 0000-0002-6016-3317; Christophe Detrembleur 0000-0001-7849-6796; Jean-Christophe M. Monbaliu 0000-0001-6916-8846;